



Biological correlates of tumor perfusion and its heterogeneity in newly diagnosed breast cancer using dynamic first-pass ^{18}F -FDG PET/CT

Neree Payan¹ · Benoit Presles¹ · François Brunotte¹ · Charles Coutant² · Isabelle Desmoulins³ · Jean-Marc Vrigneaud^{1,4} · Alexandre Cochet^{1,4}

Received: 3 April 2019 / Accepted: 1 July 2019 / Published online: 8 August 2019
© Springer-Verlag GmbH Germany, part of Springer Nature 2019

Abstract

Purpose The aim of this prospective study is to analyze the global tumor blood flow (BF) and its heterogeneity in newly diagnosed breast cancer (BC) according to tumor biological characteristics and molecular subtypes. These perfusion parameters were compared to those classically derived from metabolic studies to investigate links between perfusion and metabolism.

Methods Two hundred seventeen newly diagnosed BC patients underwent a ^{18}F -FDG PET/CT exam before any treatment. A 2-min dynamic acquisition, centered on the chest, was performed immediately after intravenous injection of 3 MBq/kg of ^{18}F -FDG, followed by a two-step static acquisition 90 min later. Tumor BF was calculated (in ml/min/g) using a single compartment kinetic model. In addition to standard PET parameters, texture features (TF) describing the heterogeneity of tumor perfusion and metabolism were extracted. Patients were divided into three groups: Luminal (HR+/HER2-), HER2 (HER2+), and TN (HR-/HER2-). Global and TF parameters of BF and metabolism were compared in different groups of patients according to tumor biological characteristics.

Results Tumors with lymph node involvement showed a higher perfusion, whereas no significant differences in SUV_{max} or SUV_{mean} were reported. TN tumors had a higher metabolic activity than HER2 and luminal tumors but no significant differences in global BF values were noted. HER2 tumors exhibited a larger tumor heterogeneity of both perfusion and metabolism compared to luminal and TN tumors. Heterogeneity of perfusion appeared well correlated to that of metabolism.

Conclusions The study of breast cancer perfusion shows a higher BF in large tumors and in tumors with lymph node involvement, not paralleled by similar modifications in tumor global metabolism. In addition, the observed correlation between the perfusion heterogeneity and the metabolism heterogeneity suggests that tumor perfusion and consequently the process of tumor angiogenesis might be involved in the metabolism heterogeneity previously shown in BC.

Keywords Breast cancer · ^{18}F -FDG PET/CT · Blood flow · Heterogeneity · Textural features

This article is part of the Topical Collection on Oncology – Chest

✉ Neree Payan
nerea.payan@u-bourgogne.fr

- ¹ ImViA EA 7535, University of Burgundy, Dijon, France
- ² Department of Surgical Oncology, Georges-François Leclerc Cancer Center, Dijon, France
- ³ Department of Medical Oncology, Georges-François Leclerc Cancer Center, Dijon, France
- ⁴ Department of Nuclear Medicine, Georges-François Leclerc Cancer Center, Dijon, France

Introduction

Breast cancer (BC) is the most common cancer and the second leading cause of death by cancer among women. This cancer has various molecular subtypes that differ in aggressiveness, treatment, and outcome [39, 52]. As a great heterogeneity regarding genetic profile, aggressiveness, and therapeutic options [43] persist, it appears essential to develop additional diagnostic tools to better characterize tumors and to guide therapeutic strategies, using biology, next-generation sequencing, and imaging. Tumors are often associated with an increase in glucose metabolism [31]

and in the context of BC, baseline metabolism is positively associated with tumor aggressiveness [15]. Beyond glucose metabolism, tumors have an increased blood flow (BF), due to the angiogenesis [35]. Since a mismatch between tumor metabolism and tumor blood flow has been reported [30], evaluation of these two different parameters appears essential to fully characterize breast tumors. Different imaging modalities, such as dynamic contrast-enhanced magnetic resonance imaging (MRI), ^{15}O -water positron emission tomography/computed tomography (PET/CT) and 1-h dynamic ^{18}F -fluorodeoxyglucose (^{18}F -FDG) PET/CT, have yielded kinetic parameters reflecting vascular permeability and perfusion. Methods based on the 2-min half-life ^{15}O remain the gold standard for perfusion evaluation [25]. However, because an on-site cyclotron is needed, only a restricted number of research centers are able to use ^{15}O -water. Furthermore, ^{18}F -FDG PET has become a standard for primary staging of large and locally advanced breast cancer [9] and a full 1-h dynamic ^{18}F -FDG PET acquisition allows tumor blood flow and metabolism evaluation after a single injection of ^{18}F -FDG. As a 1-h acquisition is hardly suitable in clinical routine, an alternative method allowing the measurement of the tumor blood flow from a first-pass ^{18}F -FDG PET has been developed by Mullani et al. [33]. The calculated blood flow [10, 20, 21] showed an excellent correlation with the tumor perfusion measured with ^{15}O -water [34]. In the context of BC, few studies have suggested the interest of the perfusion evaluation to monitor BC therapies and its ability to provide predictive and prognostic information [10, 13, 20, 21, 29, 46].

Recently, investigation of tumor heterogeneity using texture analysis (TA) has emerged [44, 45]. Standard PET/CT parameters combined with TA [2, 3, 19] appear promising to bring valuable information on the relationship between metabolism heterogeneity and clinical, biological parameters, tumor subtypes, or tumor aggressiveness [16, 28, 32, 44, 45]. In a similar way, the present paper hypothesizes that perfusion heterogeneity analysis might bring valuable additional information to metabolic imaging with ^{18}F -FDG PET/CT. Indeed, the reasons why tumors are heterogeneous are still largely unknown and one of the explanations could be the vascular disorders related to the anarchic nature of the tumor angiogenesis [1]. Nonetheless, although several previous studies have quantified ^{18}F -FDG uptake intratumoral heterogeneity, to the best of our knowledge, none was carried out on tumor BF heterogeneity. The first-pass ^{18}F -FDG PET/CT represents an opportunity to assess tumor perfusion in addition to tumor metabolism and to evaluate in a single exam, perfusion heterogeneity and its relation to metabolism heterogeneity.

The objective of this prospective study is to analyze the global tumor blood flow and its heterogeneity in a large cohort of 217 newly diagnosed breast cancer cases

according to tumor biological characteristics and molecular subtypes. These perfusion parameters were compared to those classically derived from metabolic studies to further investigate links between perfusion and metabolism.

Materials and methods

Patients and study design

From January 2011 to May 2017, 217 patients with newly diagnosed stage II or III BC were prospectively recruited, based on oncologists' recommendations for a ^{18}F -FDG PET/CT scan before any treatment. Patients with high glycemia (> 9 mmol/l) and unable or unwilling to undergo PET scan were excluded. The institutional review board approved this prospective study as a current-care study. The medical team documented patient non-opposition in source documents and in the information notice provided to the patient, and the need for a signature indicating informed consent was not required. Core biopsies of primary tumors were used to evaluate histological characteristics, such as histological type and tumor grade, using the Scarff–Bloom–Richardson (SBR) system [6]. Tumor, lymph nodes, metastasis, and classification of malignant tumors (TNM) were established in accordance with the 8th edition of the American Joint Committee on Cancer (AJCC) staging system [4]. Molecular markers examined included estrogen receptor (ER), progesterone receptor (PR) and HER2 expression. ER and PR status were considered positive if tumors showed at least 10% of positive cells. HER2 status was assessed by immunohistochemistry or fluorescent in situ hybridization (FISH) and graded from 0 to 3+. Scores of 3+ were considered positive. HER2 amplification confirmed by FISH was used to assess positivity in ambiguous cases (2+). Patients were classified into three groups according to their molecular subtypes: luminal (hormone receptors (HR)-positive, HER2-negative), HER2 (HER2-positive) and triple negative (TN) (HR-negative, HER2-negative).

PET-CT protocol

All images were acquired with a Gemini TruFlight PET/CT scanner (Philips Medical Systems, Eindhoven, The Netherlands) providing an axial field of view of 18 cm and a transaxial slice thickness of 4 mm. An automatic PET infusion system (Bayer Medical Care, Inc., Indianola, PA, USA) was used to inject a bolus of 3 MBq/kg of ^{18}F -FDG. Simultaneously with injection, an early first 8-min ^{18}F -FDG PET scan was performed, in a prone position and centered on the breast. A low-dose CT scan (120 kVp, automatic tube current modulation, 0.5-s rotation time, 16×1.5 mm

collimation, a pitch of 0.7) of the same region was carried out for anatomical registration and attenuation correction. The dynamic first-pass was reconstructed based on twelve 10-s frames extracted from the first 2 min of the PET acquisition. A whole-body emission and transmission scans were acquired 60 min later, in a supine position. Finally, 90 min after injection, the delayed static image was acquired in a prone position with a two-step PET/CT scan restricted to the chest. The emission acquisition time was 4 min per bed position. All the PET images were reconstructed using a first 3D-ordered subset iterative (OSEM) time of flight reconstruction technique with three iterations and 33 subsets. Images matrix sizes of 144×144 with an isotropic voxel size of 4 mm were used. The emission data were corrected for random coincidences, decay, dead time, scattering and attenuation.

Parametric images

Measurement of blood flow

The tumor blood flow measurement using dynamic PET of first-pass ^{18}F -FDG uptake is based on the one-compartment first-pass model of Mullani et al [33, 34] and has already been explained in detail in the literature [10, 33, 34].

Several volumes of interest (VOIs) were manually delineated on the early static PET image and the corresponding CT image using a dedicated workstation (Extended Brilliance Workspace 3.5; Philips): a first VOI representing the contours of the primary tumor, a second VOI into the ascending aorta, and a third VOI in the contralateral normal breast. The latter was used as a background reference. All the VOIs were superimposed on the dynamic PET image

and the time–activity curve (TAC) of the ascending aorta was then calculated. Counting rate reached a maximum when the arterial input to the tumor ceased and when the tracer had not left the region of interest (both arterial input and venous drainage were zero). This time T_m corresponds to the end of the first pass of the tracer and was visually determined on the arterial TAC. A parametric BF image (Fig. 1), containing a BF value in each tumor voxel, was then computed with in-house scripts using the vv tools [42], which are based on the Insight Segmentation and Registration Toolkit (ITK) library [51], by using the following equation:

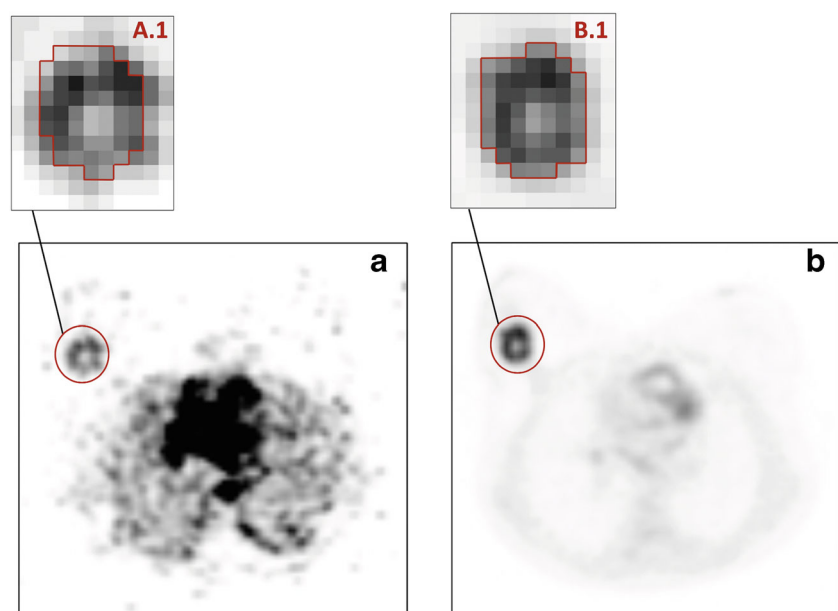
$$BF = \frac{Q(T_m)}{E \int_0^{T_m} Ca(t) dt} \quad (1)$$

where $Q(T_m)$ is the amount of tracer measured in each tumor voxel at time T_m and $Ca(t)$ is the arterial concentration of the tracer measured at time t . The extraction fraction E of ^{18}F -FDG was assumed to be equal to one [20].

Measurement of glucose metabolism

Semi-automatic segmentation using a contrast-dependent method of metabolic active tumor volumes (MATVs) were performed on the delayed static PET images. This segmentation is based on the determination of an optimal threshold value as a function of the measured contrast in the image. It requires a calibration procedure described in detail by [41]. For this purpose, phantom acquisitions were performed using the NEMA/IEC body phantom with sphere-to-background activity concentration ratios ranging from 40:1 to 2:1. These ratios were chosen to span the whole range of contrast ratios observed in the delayed PET images.

Fig. 1 Parametric blood flow (ml/min/g) image (a) from ^{18}F -FDG PET first-pass dynamic (10-s frames) acquisition and SUV image (b) from delayed (4-min per bed position) acquisition, for a 63-year-old woman with TN invasive ductal carcinoma of right breast. A.1: tumor VOI from parametric blood flow image after a rescaling using 32 grey levels. B.1: tumor VOI from SUV image after a rescaling using 64 grey levels. Primary tumor BF_{max}: 0.5, BF_{mean}: 0.2, SUV_{max}: 13.5 and SUV_{mean}: 8.1



A series of six VOIs were drawn with a distance of at least 5 mm from the spheres. The mean standardized uptake values (SUV) of all these VOIs was used as the background value. All the spheres were automatically segmented by varying a threshold in steps of 0.01. From the optimal threshold values yielding the best matching with the true spheres' volume ($\pm 2\%$), a regression function was calculated to determine the relation with the normalized thresholds and the contrast ratios, as defined in [41]. Two regression functions were used, a first one for the small volumes (less than 2 ml) and a second one for the larger volumes (more than 2 ml). The adaptive threshold algorithm was computed by using in-house tools based on the vv software. All the necrotic tumor regions were included in the tumors VOIs. Late PET images were then converted to SUV (Fig. 1) by using the classical expression:

$$SUV = \frac{\text{Tumor activity concentration (MBq/ml)}}{\text{Injected dose (MBq) / body weight (g)}} \quad (2)$$

PET-derived features

Standard PET parameters reflecting tumor metabolism and perfusion were extracted from the SUV PET and blood flow parametric images, respectively. The computed features were the average, (SUV_mean and BF_mean for the metabolism and the perfusion, respectively), the standard deviation, (SUV_sd and BF_sd) and the maximum (SUV_max and BF_max) tumor values. In addition, the metabolic active tumor volume and the total lesion glycolysis (TLG = MATV \times SUV_mean) were calculated for the metabolism. All these first-order statistics provide global information on tumor perfusion and metabolism, without any spatial information on the voxel arrangement. On the contrary, TA using second-order statistics can locally describe and quantify the spatial arrangement of the voxels. Several studies have been conducted in order to determine robust and reproducible texture features (TF) from tumor metabolic PET images [18, 27, 49] but, to the best of our knowledge, none have been conducted on the tumor perfusion images from first-pass ^{18}F -FDG PET in BC. Therefore, the same TFs were selected to study both metabolism and perfusion in order to make comparisons easier. Four TFs were used for the analysis of tumor heterogeneity: entropy, inverse different moment (IDM), correlation, and dissimilarity. The entropy is related to the orderliness in the image (how regular the pixel value differences are). This feature quantifies the randomness of the voxel intensity distribution.

$$Entropy = - \sum_{i=1}^{Nbins} \sum_{j=1}^{Nbins} P(i, j) \ln(P(i, j)) \quad (3)$$

The IDM, also called local homogeneity, quantifies the homogeneity within an image and will be high if the intensities of each pair of voxels are similar.

$$Inverse\ different\ moment = \sum_{i=1}^{Nbins} \sum_{j=1}^{Nbins} \frac{P(i, j)}{1 + (i - j)^2} \quad (4)$$

The correlation measures the linear dependency of grey levels and the dissimilarity quantifies the variation of grey-level voxel pairs.

$$Correlation = \sum_{i=1}^{Nbins} \sum_{j=1}^{Nbins} \frac{P(i, j)(i - \mu_i)(j - \mu_j)}{\sigma_i \sigma_j} \quad (5)$$

$$Dissimilarity = \sum_{i=1}^{Nbins} \sum_{j=1}^{Nbins} P(i, j) |i - j| \quad (6)$$

These features were computed in 3D using grey-level co-occurrence matrices (GLCM), which take into account pairs of voxels arrangement. For each of the 13 spatial directions, a GLCM matrix was computed between consecutive voxels (i.e., a 1-distance relationship). $P(i, j)$ is the probability value recorded for a pair of voxels in the co-occurrence matrix, μ_i and μ_j correspond to the averages on row i and column j , σ_i and σ_j are the variances on row i and column j and $Nbins$ is the number of grey levels used in the image quantization. The TF values were calculated for each matrix and then averaged to obtain the final TF values.

All the texture parameters were calculated with a fixed number of 64 bins for the metabolism analysis as recommended in the literature [17, 18, 47, 49], and with a number of 32 bins for the perfusion analysis, to minimize the impact of the noise which is higher in parametric blood flow than in metabolic images. Original PET images were rescaled between the minimum and the maximum intensity within the tumor VOI (a relative rescaling) (Fig. 1).

Statistical analysis

Statistical analysis was performed with R [40]. For all the features extracted from the parametric images, average, median, and standard deviation values were calculated. Shapiros' test was used to test the normality of the variable distribution. Since most distributions were not normal, relations between features and phenotypes were assessed using the Kruskal–Wallis test, considering a significance level of 0.05. If statistical significance was found, pairwise comparisons using a Mann–Whitney test with a Bonferroni adjustment was computed to find out differences between phenotypes. Associations between PET features and clinical and physiological parameters were investigated using a

two-sided Mann–Whitney test. Correlations between PET features were evaluated with the Spearman rank test.

Results

Patient characteristics

The study was conducted on 217 patients with a median age of 49 years and an average primary tumor diameter of 34.5 mm. The median MATV was 6.1 ml with an interquartile range of 8.2 ml and the median perfused volume was 4.0 ml with an interquartile range of 7.1 ml. Ductal carcinoma represented 93.6% of the patients, 5.5% were lobular, and 0.9% were not classified. Seventy-nine patients were HER2-positive, 81 luminal/HER2-negative, and 57 had TN tumors. Patient and tumor characteristics are summarized in Table 1.

Correlation between PET features

Figure 2 shows the Spearman correlation heat map of PET features (metabolism and perfusion). Regarding perfusion features, BF_correlation, BF_entropy and BF_IDM were strongly correlated with each other ($r > 0.74$), whereas BF_dissimilarity was inversely correlated with the other perfusion textural features ($r < -0.71$). Except for a weak correlation between BF_max and BF_entropy ($r = 0.61$), BF_max and BF_mean were not correlated with perfusion textural features. Concerning metabolic features, M_correlation, M_IDM and M_entropy were strongly correlated with each other ($r > 0.70$) and with MATV ($r > 0.73$) and TLG, whereas M_dissimilarity was strongly inversely correlated with the other metabolic textural features, MATV, and TLG. SUV_max and SUV_mean were not correlated with the other metabolic features. Regarding the correlation between perfusion and metabolic features, except for a weak correlation between BF_max and TLG ($r = 0.64$), there was no significant correlation between standard metabolism features (SUV_max, SUV_mean, MATV, TLG) and perfusion standard features (BF_max and BF_mean). In contrast, BF_correlation, BF_entropy and BF_IDM were correlated with M_correlation, M_entropy, MATV, and TLG, and inversely correlated with M_dissimilarity. Finally, BF_dissimilarity was correlated with M_dissimilarity and inversely correlated with the other metabolic TFs.

Relationship between PET-derived features and tumor characteristics

Table 2 summarizes the PET-derived features in association with the tumor characteristics. Concerning perfusion parameters, there was no difference according to ER, PR, and HER2 status. In contrast, BF_max, BF_entropy and

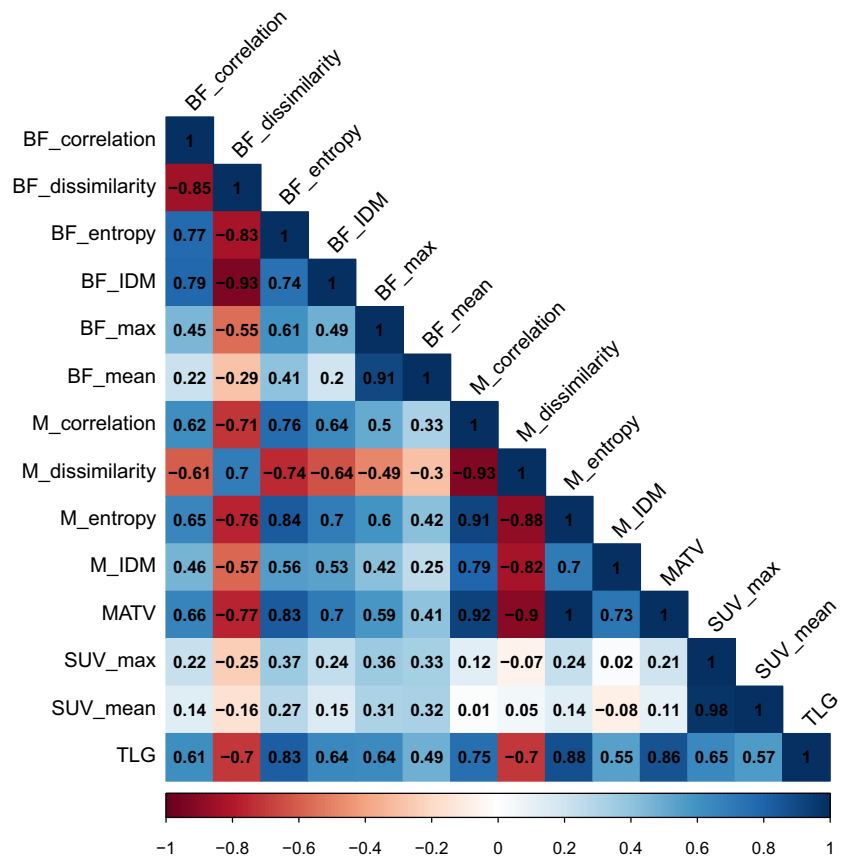
Table 1 Patient and tumor characteristics

	Number of patients (%) <i>N</i> = 217
Menopausal	
Yes	93 (42.9)
No	124 (57.1)
T stage	
T1	23 (10.6)
T2	150 (69.1)
T3	12 (5.5)
T4	32 (14.8)
N stage	
N0	74 (34.1)
N1	104 (47.9)
N2	20 (9.2)
N3	19 (8.8)
SBR	
Grade 1 and 2	115 (53)
Grade 3	102 (47)
Histological type	
Ductal	203 (93.6)
Lobular	12 (5.5)
Others	2 (0.9)
ER status	
Positive	124 (57.1)
Negative	93 (42.9)
PR status	
Positive	91 (41.9)
Negative	126 (58.1)
HER2 status	
Positive	79 (36.4)
Negative	138 (63.6)
Breast cancer sub-group	
ER+/HER2-	81 (37.3)
HER2+	79 (36.4)
TN	57 (26.3)

ER: estrogen receptor; PR: progesterone receptor; TN: triple negative

BF_correlation were significantly higher in the event of T stage 3–4, lymph node involvement or ductal carcinoma, whereas BF_dissimilarity was lower. T stage 3–4 tumors also exhibited higher BF_IDM. Finally, BF_max was higher for SBR grade III. Regarding metabolic features, both SUV_max and SUV_mean were significantly higher in the event of SBR grade III, ductal carcinoma, ER negative, and PR negative. In contrast, no differences were found for SUV_max and SUV_mean concerning HER2 status, T-stage and N-stage. Higher MATV and TLG were found in patients with T-stage 3–4, N⁺ status, and with HER2-status. TLG was also higher in the event of SBR grade III and ductal carcinoma. M_entropy, M_IDM and M_correlation

Fig. 2 Spearman rank correlation heat map between blood flow texture features, metabolism texture features, and standard PET features. The *dark blue colors* represent strong positive correlations (close to 1), the *dark red* represent strong inverse correlations (close to -1). The *light/white* represent an absence of correlation (close to 0). BF: blood flow; IDM: inverse different moment; M: metabolism; MATV: metabolic active tumor volume; SUV: standardized uptake value; TLG: total lesion glycolysis



were higher in patients with T-stage 3–4 and HER2 negative, whereas M_{dissimilarity} was lower. M_{entropy} and M_{correlation} were also higher in patients with N⁺ status.

Comparison between phenotypes

Table 3, Figs. 3, and 4 summarize the comparison of blood flow and metabolism characteristics between BC phenotypes. Regarding global BF analysis, no significant differences among phenotypes were observed. TF analysis showed no significant differences between HER2 and Luminal tumors. However, TN tumors had a significantly higher entropy than luminal tumors (entropy: TN = 6.18 ± 1.65 , luminal = 5.49 ± 1.45 , $p=0.011$), and a significantly higher homogeneity than the HER2 ones (IDM: HER2 = 0.14 ± 0.05 , TN = 0.17 ± 0.06 , $p=0.015$; correlation: HER2 = 0.29 ± 0.22 , TN = 0.37 ± 0.23 , $p=0.034$). Concerning metabolism analysis, TN tumors showed higher values of SUV_{max} and SUV_{mean} than HER2 and luminal tumors. In addition, TF analysis showed that HER2 tumors had a significantly lower homogeneity and entropy than luminal tumors (IDM: HER2 = 0.06 ± 0.02 , luminal = 0.07 ± 0.02 , $p<0.001$; entropy: HER2 = 6.22 ± 1.53 , luminal = 6.80 ± 1.59 , $p=0.034$). HER2 tumors had also a lower homogeneity and entropy than TN ones (IDM: TN

= 0.07 ± 0.03 , entropy: TN = 6.86 ± 1.93 , $p=0.023$ and $p=0.047$). No significant differences in heterogeneity were reported between TN and luminal tumors.

Discussion

The present paper shows that adding blood flow evaluation, from the first pass of ¹⁸F-FDG, to the more conventional delayed ¹⁸F-FDG uptake, brings new insights into breast cancer biology. Global blood flow increases in the context of large tumors and axillary lymph node invasion. Texture analysis shows that perfusion heterogeneity parallels that of metabolism. These results suggest a complementary role of advanced textural features and standard PET imaging parameters for the in vivo biological characterization of BC lesions, supporting the hypothesis that advanced PET imaging analysis can provide additional information.

As previously reported, global tumor perfusion was found to be almost identical in the three BC subtypes [20, 46], while glucose uptake significantly increased from luminal to HER2 and TN tumors [9, 10, 15, 16, 20, 32]. The increased metabolism of some tumors, especially the TN subtype, has led to the mismatch concept between perfusion and tumor metabolism [10]. Regarding the

Table 2 Relationship between PET-derived features, histological factors, and tumor characteristics (Mann–Whitney *p* values). The average of the feature values for each group is presented in parentheses when significant

PET features	T stage 1-2 vs. 3-4	N stage 0 vs. 1-3	SBR 1-2 vs. 3	Histology ductal vs. lobular	Estrogen receptor - vs. +	Progesterone receptor - vs. +	HER2 status - vs. +
Blood flow							
BF,max (ml/min/g)	0.03 (0.33 vs. 0.46)	0.001 (0.29 vs. 0.40)	0.036 (0.33 vs. 0.39)	<0.001 (0.37 vs. 0.18)	0.10	0.18	0.69
BF,mean (ml/min/g)	0.063	<0.001 (0.13 vs. 0.19)	0.07	0.006 (0.18 vs. 0.11)	0.24	0.23	0.79
Entropy	<0.001 (5.55 vs. 6.41)	0.002 (5.27 vs. 5.96)	0.06	0.009 (5.77 vs. 4.62)	0.14	0.18	0.54
IDM	0.002 (0.15 vs. 0.17)	0.21	0.41	0.07	0.85	0.80	0.054
Dissimilarity	<0.001 (7.24 vs. 5.96)	0.020 (7.5 vs. 6.7)	0.21	0.029 (6.91 vs. 8.48)	0.81	0.87	0.22
Correlation	0.023 (0.29 vs. 0.38)	0.013 (0.26 vs. 0.34)	0.49	0.01 (0.32 vs. 0.16)	0.94	0.96	0.16
SUV,max	0.30	0.06	<0.001 (7.7 vs. 13.2)	<0.001 (10.6 vs. 4.6)	<0.001 (12.4 vs. 8.6)	<0.001 (11.7 vs. 8.2)	0.84
SUV,mean	0.16	0.08	<0.001 (4.7 vs. 7.8)	<0.001 (6.3 vs. 3.0)	<0.001 (7.3 vs. 5.3)	<0.001 (7.0 vs. 5.0)	0.71
MATV	<0.001 (9.45 vs. 19.21)	<0.001 (6.8 vs. 13.8)	0.44	0.22	0.22	0.43	0.003 (13.9 vs. 7.2)
TLG	0.012 (66.5 vs. 127.6)	<0.001 (40.9 vs. 98.6)	<0.001 (51.8 vs. 110.0)	0.004 (82.4 vs. 19.4)	0.27	0.17	0.025 (97.8 vs. 45.9)
Entropy	<0.001 (6.38 vs. 7.49)	<0.001 (6.1 vs. 6.9)	0.31	0.18	0.25	0.45	0.004 (6.83 vs. 6.22)
IDM	<0.001 (0.06 vs. 0.08)	0.37	0.91	0.97	0.13	0.39	<0.001 (0.070 vs. 0.056)
Dissimilarity	<0.001 (17.9 vs. 14.6)	0.06	0.89	0.84	0.11	0.25	0.002 (16.5 vs. 18.4)
Correlation	<0.001 (0.16 vs. 0.32)	0.001 (0.13 vs. 0.22)	0.55	0.70	0.082 (0.17 vs. 0.21)	0.15	0.004 (0.22 vs. 0.14)

BF: blood flow; IDM: inverse different moment; MATV: metabolic active tumor volume; SUV: standardized uptake value; TLG: total lesion glycolysis

Table 3 Comparison between blood flow and metabolism characteristics for each breast cancer phenotype

	PET features	BC subgroups values			BC subgroups comparison		
		Luminal (mean ± sd)	HER2 (mean ± sd)	TN (mean ± sd)	Luminal-HER2 (<i>p</i> value)	Luminal-TN (<i>p</i> value)	HER2-TN (<i>p</i> value)
Blood flow	BF.max (ml/min/g)	0.32±0.19	0.37±0.29	0.40±0.21	–	–	–
	BF.mean (ml/min/g)	0.17±0.09	0.18±0.12	0.18±0.08	–	–	–
	Entropy	5.49±1.45	5.62±1.47	6.18±1.65	–	0.011	–
	IDM	0.15±0.05	0.14±0.05	0.17±0.06	–	–	0.015
	Dissimilarity	7.07±2.21	7.20±2.41	6.53±2.61	–	–	–
	Correlation	0.29±0.23	0.29±0.22	0.37±0.23	–	–	0.034
Metabolism	SUV_max	8.0±5.0	10.0±5.1	13.8±6.8	0.020	<0.001	0.006
	SUV_mean	4.9±3.0	6.1±3.1	8.0±3.8	0.021	<0.001	0.018
	TLG	56.1±87.0	45.9±61.7	157.2±362.7	–	0.033	0.003
	Entropy	6.80±1.59	6.22±1.53	6.86±1.93	0.034	–	0.047
	IDM	0.07±0.02	0.06±0.02	0.07±0.03	<0.001	–	0.023
	Dissimilarity	16.5±4.0	18.4±3.8	16.6±5.3	0.008	–	–
	Correlation	0.22±0.19	0.14±0.19	0.21±0.25	0.014	–	–

BF: blood flow; IDM: inverse different moment; TLG: total lesion glycolysis

relationship between global perfusion parameters and tumor characteristics, no association between blood flow average (BF_mean) and hormonal receptors or SBR was observed, as previously reported [10, 20, 32]. Although no perfusion difference was highlighted in a previous paper from our institution [20], a significantly higher perfusion was however noted, in the present study, for ductal carcinomas. The larger number of patients here (217 vs. 150) may potentially explain this difference in the results. As there is an important numeric disproportion between the lobular and the ductal tumor population, results must be carefully interpreted. However, the observation of a higher perfusion for ductal carcinomas is in line with some previous studies where the expression of vascular endothelial growth factor (VEGF) protein was significantly higher in invasive ductal carcinomas than in invasive lobular carcinomas [11, 26].

Moreover, in the present study, T3-T4 tumors were found to have a higher BF_max than T1-T2 tumors and this observation has not been reported before. It could be argued that tumor blood flow increases with size but the blood flow “max” is calculated within a small part of a tumor, i.e., a cube of 64 mm³ representing less than 100 mg of tumor. Yet, this observation is in line with a recent study [23] where a significantly lower microvessel density was associated with a smaller tumor size. Fifty percent of tumors with a diameter between 2 and 5 cm had a microvessel density > 72.9/mm² by comparison to only 38% in tumors with a diameter smaller than 2 cm. Moreover, we noted that, in patients with lymph nodes involvement (N⁺), primary tumors also exhibited a

higher BF. Lymph node involvement reflects tumor local invasion and is an important prognostic factor. Similarly, a borderline correlation has been reported [5] between vascular proliferation index and positive nodal status in a series of 110 patients with locally advanced breast cancer. Supporting these observations, a color Doppler ultrasound study showed in a large cohort of breast carcinomas (368 patients) that the peak systolic flow velocity was significantly associated with tumor size and the presence of axillary lymph node metastases [7]. In the same way, a direct association has also been reported between expression of VEGF and the tumor size and the number of metastatic lymph nodes [11].

The differences observed in perfusion depending on tumor size and lymph node involvement might reflect an increased angiogenesis. Indeed, it has been suggested that angiogenesis in breast cancer is regulated by vascular factors secreted by tumor cells and has a close relationship with axillary nodule metastasis [8]. Angiogenesis plays an important role in both tumor growth and metastasis of many types of cancers and is recognized as an important hallmark of oncogenesis [14]. This might provide an explanation to the higher perfusion observed in primary tumors with clinical lymph node involvement, as extensive angiogenesis could facilitate cancer metastasis. These differences in perfusion according to T-stage and N-stage are not paralleled by similar differences in tumor metabolism, as no significant differences were noted for both SUV_max or SUV_mean. This observation might suggest that studying perfusion might provide further insights in breast cancer invasiveness.

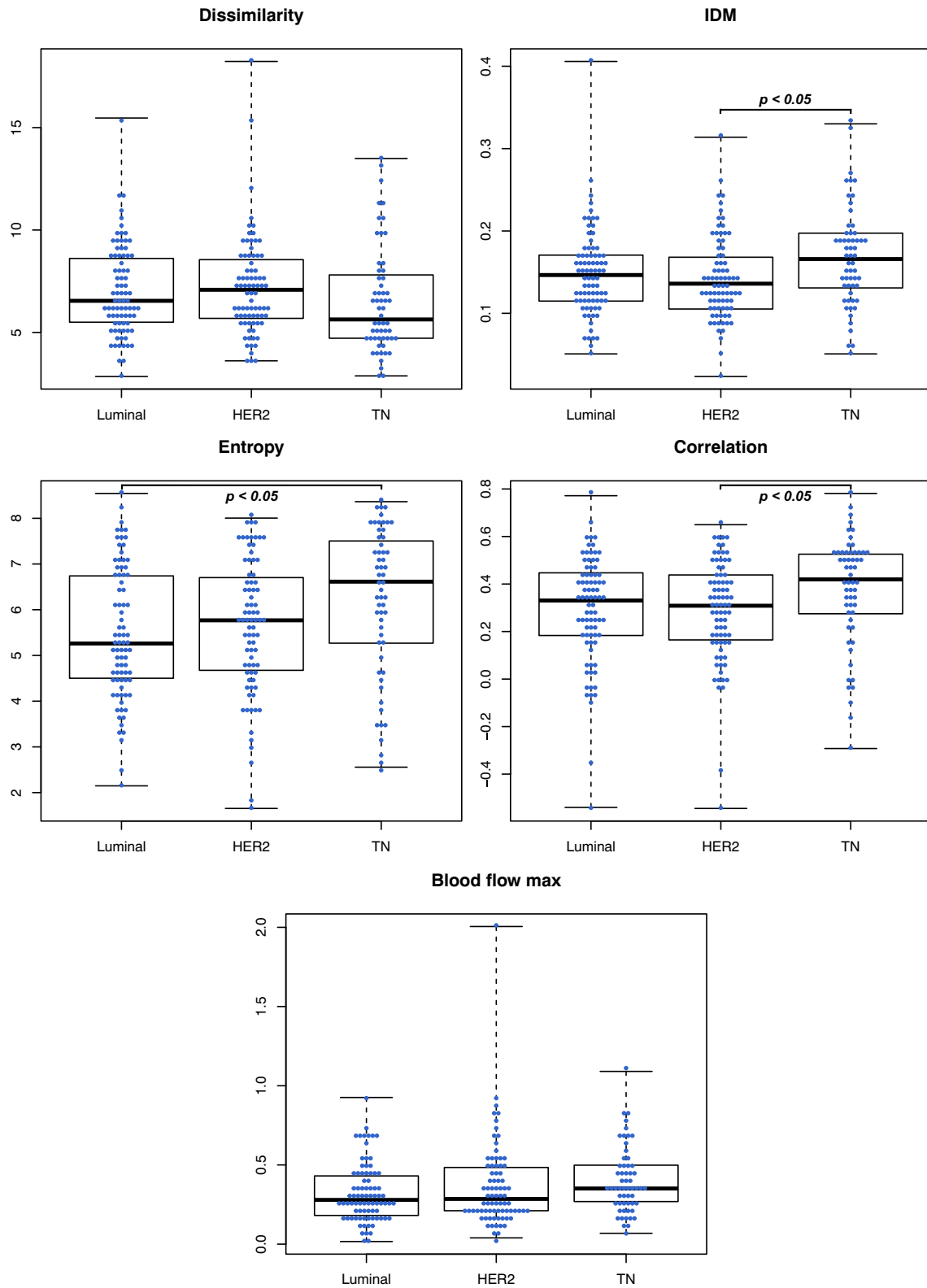


Fig. 3 Distribution of PET features among phenotypes for blood flow. IDM: inverse different moment

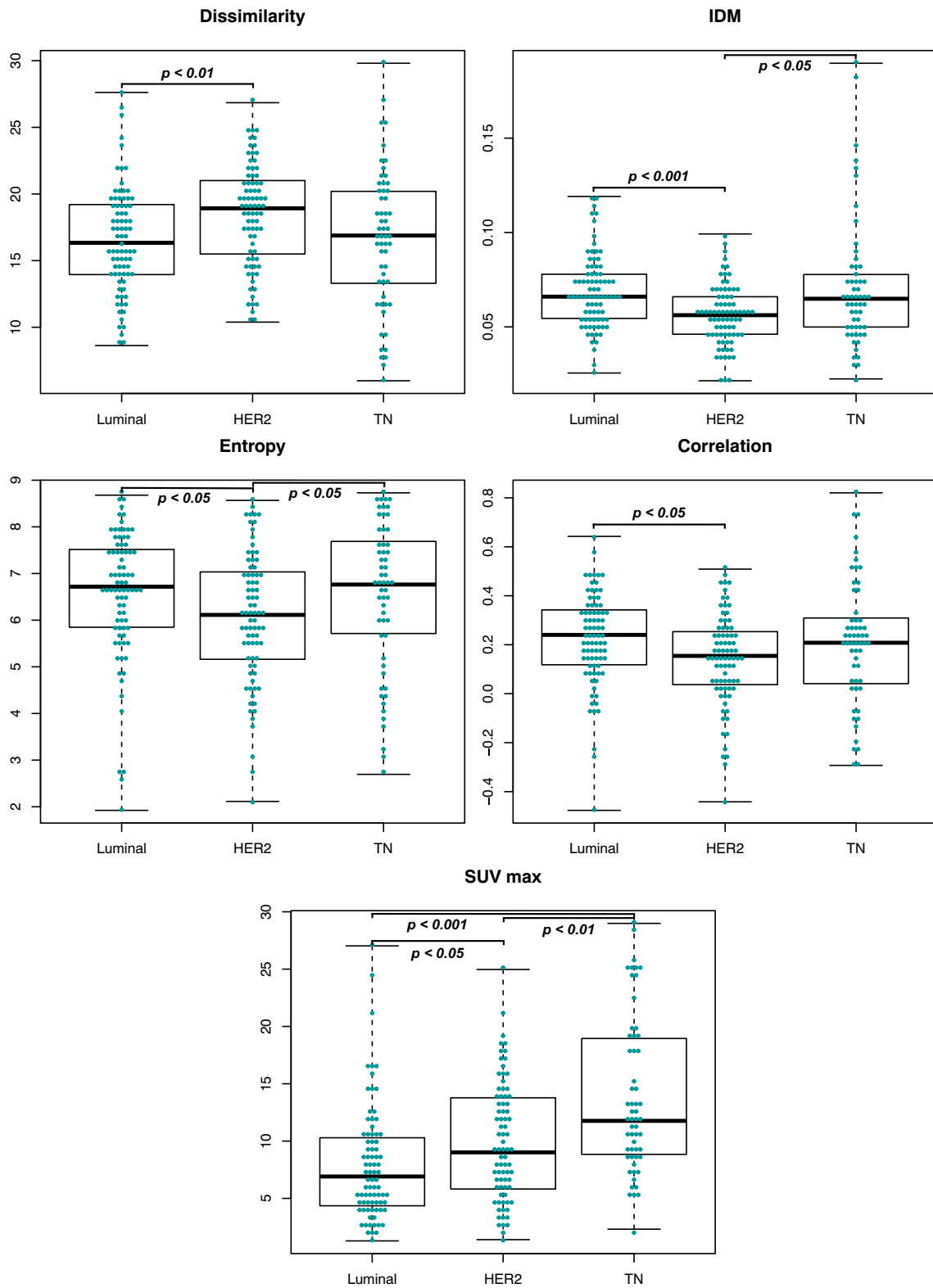


Fig. 4 Distribution of PET features among phenotypes, for metabolism. IDM: inverse different moment; SUV: standardized uptake value

In recent years, several studies have investigated the heterogeneity of ^{18}F -FDG uptake in different tumor types. Some research has focused on breast cancer and various image-derived features, reflecting heterogeneity, have been proposed. Most of these studies have been mainly descriptive, attempting to find correlations with tumor subtypes and treatment responses. In the present study, using a single ^{18}F -FDG PET/CT exam, we were able to characterize both tumor perfusion and metabolism heterogeneity and look for possible links between these two tumor hallmarks' heterogeneity. Texture feature interpretation can be influenced by the method used to calculate it. Depending on the PET image rescaling method [27, 37], it was shown that the texture feature will not have the same behavior, and potentially not the same meaning [27, 28, 36–38]. Bearing this question in mind, a limited number of texture features known to be robust and reproducible [17, 19, 28, 37, 38, 49] were selected in the present study. Moreover, similar texture features were used to study both perfusion and metabolism, thus making comparisons easier.

To the best of our knowledge, no prior study has addressed perfusion heterogeneity using PET/CT in BC. Among a large population covering different BC phenotypes, the differences found between HER2 and TN tumors were significant, with a higher heterogeneity in the HER2 subtype. This difference was also found between HER2 tumors and luminal tumors, but was not significant. Metabolism heterogeneity analysis highlighted similar differences between phenotypes, with HER2 tumors significantly more heterogeneous than luminal and TN tumors. Consequently, HER2 subtype appeared here, as the most heterogeneous phenotype, in both perfusion and metabolism. It is worth noting that perfusion heterogeneity matched metabolism heterogeneity.

One possible interpretation of these facts might be related to the heterogeneous distribution of vascular density within the tumor, due to angiogenesis [1]. Indeed, previous published works underlined the relationship between the HER2-positive tumors and angiogenesis [22, 24, 50]. Moreover, for this BC subtype, clinical trials have suggested that addition of an antiangiogenic treatment to a conventional neoadjuvant chemotherapy, can increase the proportion of patients who achieve a pathological complete response [12], supporting the link between HER2 and angiogenesis.

Finally, unlike global perfusion parameters that show only a limited correlation with standard metabolism features [10, 46], perfusion TFs and metabolism TFs were highly correlated (for example, $r=0.84$ for the correlation between Mentropy and BF.entropy). As the heterogeneity is assessed by comparison of neighbor pixels, this could reflect some anarchic distribution of perfusion and metabolism. One study has investigated the heterogeneity of microvessels in

BC [1] at the microscopic level. The authors concluded that heterogeneity is even more important inside a given tumor than among various types of tumors. Results obtained here may suggest that understanding perfusion heterogeneity at the pixel level could possibly be a step forward in the comprehension of metabolism heterogeneity.

Study limitations

One of the main limitations of this study is the small volume of the tumors. However, small tumor size is one of breast cancer's characteristics and the choice of TFs was done taking into account this aspect, using local TFs only. Considering the wide range of techniques available and the contradictory results, a careful interpretation of heterogeneity should be done. Regarding perfusion and metabolism tumor heterogeneities comparison, we performed a global rather than a voxel-to-voxel comparison given that perfusion and metabolism were evaluated from two different acquisitions.

No correction for partial volume effect was applied and the low count statistics in the dynamic images might add a bias that could affect the results [48]. By improving the signal-to-noise ratio and the spatial resolution of the dynamic short time frames, better image quality should be obtained, leading to new or more significant results. Improvement of spatial resolution and sensitivity provided by new digital PET or dedicated breast PET scanners should improve the analysis in this range of tumor sizes. Moscoso et al. [32] recently investigated the dedicated breast PET resolution improvement. They showed that this technique enables a more accurate heterogeneity characterization, but they focused only on metabolism analysis.

Conclusions

In this study, a significantly higher perfusion in tumors with lymph node involvement has been highlighted, whereas no significant difference was noted in tumor metabolism. In addition, tumor blood flow heterogeneity was different in different breast cancer phenotypes and this was not previously observed with a global analysis of the perfusion. A combination of standard PET parameters and textural features of both tumor perfusion and metabolism could represent a step forward towards a better understanding of tumor behavior and therapeutic strategies adaptation, in the era of personalized medicine. The next step would be to investigate if all these new texture features and their early changes during therapy might improve clinical outcome prediction or treatment response, as potential biomarkers of therapeutic response.

Acknowledgements The authors thank the technologists from the Department of Nuclear Medicine of the Georges-François Leclerc Center for their help in the development of this study, Genevieve Laporte for her help with the clinical database, and Isabel Gregoire for the English revision of the manuscript.

Compliance with Ethical Standards

Conflict of interest The authors declare that they have no conflicts of interest.

Ethical approval This study was conducted in accordance with the Declaration of Helsinki and approved by the institutional ethics committee of the Georges-François Leclerc Center.

Informed consent The patient non-opposition was recorded in source documents by the medical team and used as patient informed consent.

References

- Ahlgren J, Risberg B, Villman K, Bergh J. Angiogenesis in invasive breast carcinoma—a prospective study of tumour heterogeneity. *Eur J Cancer*. 2002;38(1):64–69.
- Alic L, Niessen WJ, Veenland JF. Quantification of heterogeneity as a biomarker in tumor imaging: a systematic review. *PLoS One*. 2014;9(10):e110,300.
- Amadasun M, King R. Textural features corresponding to textural properties. *IEEE Trans Syst Man Cybern*. 1989;19(5):1264–1274.
- Amin MB, Edge SB, Greene FL, Byrd DR, Brookland RK, Washington MK, Gershenwald JE, Compton CC, Hess KR, Sullivan DC, Milburn Jessup J, Brierley JD, Gaspar LE, Schilsky RL, Balch CM, Winchester DP, Asare EA, Madera M, Gress DM, Meyer LR. *AJCC Cancer Staging Manual*. Springer. 2018.
- Arnes JB, Stefansson IM, Straume O, Baak JP, Lønning PE, Foulkes WD, Akslen LA. Vascular proliferation is a prognostic factor in breast cancer. *Breast Cancer Res Treat*. 2012;133(2):501–510.
- Bhargava R, Striebel J, Beriwal S, Flickinger JC, Onisko A, Ahrendt G, Dabbs DJ. Prevalence, morphologic features and proliferation indices of breast carcinoma molecular classes using immunohistochemical surrogate markers. *Int J Clin Exp Pathol*. 2009;2(5):444.
- Chao TC, Luo YF, Chen SC, Chen MF. Color Doppler ultrasound in breast carcinomas: relationship with hormone receptors, DNA ploidy, s-phase fraction, and histopathology. *Ultrasound Med Biol*. 2001;27(3):351–355.
- Choi WWL, Lewis MM, Lawson D, Yin-Goen Q, Birdsong GG, Cotsonis GA, Cohen C, Young AN. Angiogenic and lymphangiogenic microvessel density in breast carcinoma: correlation with clinicopathologic parameters and VEGF-family gene expression. *Mod Pathol*. 2005;18(1):143–152.
- Cochet A, Dygai-Cochet I, Riedinger JM, Humbert O, Berriolo-Riedinger A, Toubreau M, Guiu S, Coutant C, Coudert B, Fumoleau P, Brunotte F. 18F-FDG PET/CT provides powerful prognostic stratification in the primary staging of large breast cancer when compared with conventional explorations. *Eur J Nucl Med Mol Imaging*. 2013;41(3):428–437.
- Cochet A, Pigeonnat S, Khoury B, Vrigneaud JM, Touzery C, Berriolo-Riedinger A, Dygai-Cochet I, Toubreau M, Humbert O, Coudert B, Fumoleau P, Arnould L, Brunotte F. Evaluation of breast tumor blood flow with dynamic first-pass 18F-FDG PET/CT: comparison with angiogenesis markers and prognostic factors. *J Nucl Med*. 2012;53(4):512–520.
- Coradini D, Pellizzaro C, Veneroni S, Ventura L, Daidone MG. Infiltrating ductal and lobular breast carcinomas are characterised by different interrelationships among markers related to angiogenesis and hormone dependence. *Br J Cancer*. 2002;87(10):1105–1111.
- Coudert B, Pierga JY, Mouret-Reynier MA, Kerrou K, Ferrero JM, Petit T, Kerbrat P, Dupré PF, Bachelot T, Gabelle P, Giard S, Coeffic D, Bougnoux P, Prevost JB, Pintaud G, Thibault G, Hernandez J, Coudert M, Arnould L, Berriolo-Riedinger A. Use of [18F]-FDG PET to predict response to neoadjuvant trastuzumab and docetaxel in patients with HER2-positive breast cancer, and addition of bevacizumab to neoadjuvant trastuzumab and docetaxel in [18F]-FDG PET-predicted non-responders (AVATAXHER): an open-label, randomised phase 2 trial. *Lancet Oncol*. 2014;15(13):1493–1502.
- Dunnwald LK, Gralow JR, Ellis GK, Livingston RB, Linden HM, Specht JM, Doot RK, Lawton TJ, Barlow WE, Kurland BF, Schubert EK, Mankoff DA. Tumor metabolism and blood flow changes by positron emission tomography: relation to survival in patients treated with neoadjuvant chemotherapy for locally advanced breast cancer. *J Clin Oncol*. 2008;26(27):4449–4457.
- Folkman J. Tumor angiogenesis: therapeutic implications. *N Engl J Med*. 1971;285(21):1182–1186.
- Groheux D, Giacchetti S, Moretti JL, Porcher R, Espié M, Lehmann-Che J, de Roquancourt A, Hamy AS, Cuvier C, Vercellino L, Hindié E. Correlation of high 18F-FDG uptake to clinical, pathological and biological prognostic factors in breast cancer. *Eur J Nucl Med Mol Imaging*. 2011;38(3):426–435.
- Groheux D, Majdoub M, Tixier F, Le Rest CC, Martineau A, Merlet P, Espié M, de Roquancourt A, Hindié E, Hatt M, Visvikis D. Do clinical, histological or immunohistochemical primary tumour characteristics translate into different (18)F-FDG PET/CT volumetric and heterogeneity features in stage II/III breast cancer. *Eur J Nucl Med Mol Imaging*. 2015;42(11):1682–1691.
- Hatt M, Majdoub M, Vallières M, Tixier F, Le Rest CC, Groheux D, Hindié E, Martineau A, Pradier O, Hustinx R, Perdrisot R, Guillemin R, El Naqa I, Visvikis D. 18F-FDG PET uptake characterization through texture analysis: investigating the complementary nature of heterogeneity and functional tumor volume in a multi-cancer site patient cohort. *J Nucl Med*. 2015;56(1):38–44.
- Hatt M, Tixier F, Le Rest CC, Pradier O, Visvikis D. Robustness of intratumour 18F-FDG PET uptake heterogeneity quantification for therapy response prediction in oesophageal carcinoma. *Eur J Nucl Med Mol Imaging*. 2013;40(11):1662–1671.
- Hatt M, Tixier F, Pierce L, Kinahan PE, Le Rest CC, Visvikis D. Characterization of PET/CT images using texture analysis: the past, the present any future. *Eur J Nucl Med Mol Imaging*. 2017;44(1):151–165.
- Humbert O, Lasserre M, Bertaut A, Fumoleau P, Coutant C, Brunotte F, Cochet A. Breast cancer blood flow and metabolism on dual-acquisition 18F-FDG PET: correlation with tumor phenotype and neoadjuvant chemotherapy response. *J Nucl Med*. 2018;59(7):1035–1041.
- Humbert O, Riedinger JM, Vrigneaud JM, Kanoun S, Dygai-Cochet I, Berriolo-Riedinger A, Toubreau M, Depardon E, Lasserre M, Tisserand S, Fumoleau P, Brunotte F, Cochet A. 18F-FDG PET-derived tumor blood flow changes after 1 cycle of neoadjuvant chemotherapy predicts outcome in triple-negative breast cancer. *J Nucl Med*. 2016;57(11):1707–1712.
- Konecny GE, Meng YG, Untch M, Wang HJ, Bauerfeind I, Epstein M, Stieber P, Vernes JM, Gutierrez J, Hong K, Beryt M, Hepp H, Slamon DJ, Pegram MD. Association between

- HER-2/neu and vascular endothelial growth factor expression predicts clinical outcome in primary breast cancer patients. *Clin Cancer Res.* 2004;10(5):1706–1716.
23. Kraby MR, Opdahl S, Russnes HG, Bofin AM. Microvessel density in breast cancer: the impact of field area on prognostic informativeness. *J Clin Pathol.* 2019.
 24. Kumar R, Yarmand-Bagheri R. The role of HER2 in angiogenesis. *Semin Oncol.* 2001;28(5 Suppl 16):27–32.
 25. Laking G, Price P. Radionuclide imaging of perfusion and hypoxia. *Eur J Nucl Med Mol Imaging.* 2010;37(S1):20–29.
 26. Lee AH, Dublin EA, Bobrow LG, Poulson R. Invasive lobular and invasive ductal carcinoma of the breast show distinct patterns of vascular endothelial growth factor expression and angiogenesis. *J Pathol.* 1998;185(4):394–401.
 27. Leijenaar RTH, Nalbantog V, Carvalho S, van Elmpt WJC, Troost EGC, Boellaard R, Aerts HJWL, Gillies RJ, Lambin P. The effect of SUV discretization in quantitative FDG-PET radiomics: the need for standardized methodology in tumor texture analysis. *Sci Rep.* 2015;5(11):075.
 28. Lemarignier C, Martineau A, Teixeira L, Vercellino L, Espié M, Merlet P, Groheux D. Correlation between tumour characteristics, SUV measurements, metabolic tumour volume, TLG and textural features assessed with F-FDG PET in a large cohort of oestrogen receptor-positive breast cancer patients. *Eur J Nucl Med Mol Imaging.* 2017;44(7):1145–1154.
 29. Mankoff DA, Dunnwald LK, Gralow JR, Ellis GK, Charlop A, Lawton TJ, Schubert EK, Tseng J, Livingston RB. Blood flow and metabolism in locally advanced breast cancer: relationship to response to therapy. *J Nucl Med.* 2002;43(4):500–509.
 30. Mankoff DA, Dunnwald LK, Partridge SC, Specht JM. Blood flow-metabolism mismatch: good for the tumor, bad for the patient. *Clin Cancer Res.* 2009;15(17):5294–5296.
 31. Mérida I, Ávila-Flores A. Tumor metabolism: new opportunities for cancer therapy. *Clin Transl Oncol.* 2006;8(10):711–716.
 32. Moscoso A, RuiBAL Á, Domínguez-Prado I, Fernández-Ferreiro A, Herranz M, Albaina L, Argibay S, Silva-Rodríguez J, Pardo-Montero J, Aguiar P. Texture analysis of high-resolution dedicated breast F-FDG PET images correlates with immunohistochemical factors and subtype of breast cancer. *Eur J Nucl Med Mol Imaging.* 2018;45(2):196–206.
 33. Mullani NA, Gould KL. First-pass measurements of regional blood flow with external detectors. *J Nucl Med.* 1983;24(7):577–581.
 34. Mullani NA, Herbst RS, O’Neil RG, Gould KL, Barron BJ, Abbruzzese JL. Tumor blood flow measured by PET dynamic imaging of first-pass 18F-FDG uptake: a comparison with 15O-labeled water-measured blood flow. *J Nucl Med.* 2008;49(4):517–523.
 35. Neufeld G, Kessler O. Pro-angiogenic cytokines and their role in tumor angiogenesis. *Cancer Metastasis Rev.* 2006;25(3):373–385.
 36. Orlhac F, Nioche C, Soussan M, Buvat I. Understanding changes in tumor texture indices in PET: a comparison between visual assessment and index values in simulated and patient data. *J Nucl Med.* 2017;58(3):387–392.
 37. Orlhac F, Soussan M, Chouahnia K, Martinod E, Buvat I. 18F-FDG PET-derived textural indices reflect tissue-specific uptake pattern in non-small cell lung cancer. *PLoS One.* 2015;10(12):e0145063.
 38. Orlhac F, Soussan M, Maisonobe JA, Garcia CA, Vanderlinden B, Buvat I. Tumor texture analysis in 18F-FDG PET: relationships between texture parameters, histogram indices, standardized uptake values, metabolic volumes, and total lesion glycolysis. *J Nucl Med.* 2014;55(3):414–422.
 39. Perou CM, Sørli T, Eisen MB, van de Rijn M, Jeffrey SS, Rees CA, Pollack JR, Ross DT, Johnsen H, Akslen LA, Fluge Ø, Pergamenschikov A, Williams C, Zhu SX, Lønning PE, Børresen-Dale AL, Brown PO, Botstein D. Molecular portraits of human breast tumours. *Nature.* 2000;406(6797):747–752.
 40. R Core Team. R: A language and environment for statistical computing. R Foundation for Statistical Computing, Vienna, Austria. 2017. <http://www.R-project.org/>.
 41. Schaefer A, Kremp S, Hellwig D, Rube C, Kirsch CM, Nestle U. A contrast-oriented algorithm for FDG-PET-based delineation of tumour volumes for the radiotherapy of lung cancer: derivation from phantom measurements and validation in patient data. *Eur J Nucl Med Mol Imaging.* 2008;35(11):1989–1999.
 42. Seroul P, Sarrut D. VV: A viewer for the evaluation of 4D image registration. *MIDAS Journal (Medical Image Computing and Computer-Assisted Intervention MICCAI’2008, Workshop - Systems and Architectures for Computer Assisted Interventions)*, 1–8. 2008. <http://vv.creatis.insa-lyon.fr/>.
 43. Shi Y, Jin J, Ji W, Guan X. Therapeutic landscape in mutational triple-negative breast cancer. *Mol Cancer.* 2018;17(1):99.
 44. Son SH, Kim DH, Hong CM, Kim CY, Jeong SY, Lee SW, Lee J, Ahn BC. Prognostic implication of intratumoral metabolic heterogeneity in invasive ductal carcinoma of the breast. *BMC Cancer.* 2014;14:585.
 45. Soussan M, Orlhac F, Boubaya M, Zelek L, Ziolo M, Eder V, Buvat I. Relationship between tumor heterogeneity measured on FDG-PET/CT and pathological prognostic factors in invasive breast cancer. *PLoS One.* 2014;9(4):e94017.
 46. Specht JM, Kurland BF, Montgomery SK, Dunnwald LK, Doot RK, Gralow JR, Ellis GK, Linden HM, Livingston RB, Allison KH, Schubert EK, Mankoff DA. Tumor metabolism and blood flow as assessed by positron emission tomography varies by tumor subtype in locally advanced breast cancer. *Clin Cancer Res.* 2010;16(10):2803–2810.
 47. Tixier F, Hatt M, Le Rest CC, Le Pogam A, Corcos L, Visvikis D. Reproducibility of tumor uptake heterogeneity characterization through textural feature analysis in 18F-FDG PET. *J Nucl Med.* 2012;53(5):693–700.
 48. Walker MD, Asselin MC, Julyan PJ, Feldmann M, Talbot PS, Jones T, Matthews JC. Bias in iterative reconstruction of low-statistics PET data: benefits of a resolution model. *Phys Med Biol.* 2011;56(4):931–949.
 49. Yan J, Chu-Shern JL, Loi HY, Khor LK, Sinha AK, Quek ST, Tham IWK, Townsend D. Impact of image reconstruction settings on texture features in 18F-FDG PET. *J Nucl Med.* 2015;56(11):1667–1673.
 50. Yang W, Klos K, Yang Y, Smith TL, Shi D, Yu D. ErbB2 overexpression correlates with increased expression of vascular endothelial growth factors A, C, and D in human breast carcinoma. *Cancer.* 2002;94(11):2855–61.
 51. Yoo TS, Ackerman MJ, Lorensen WE, Schroeder W, Chalana V, Aylward S, Metaxas D, Whitaker R. Engineering and algorithm design for an image processing API: a technical report on ITK - the insight toolkit. In: Westwood J, editor. *Proceedings of medicine meets virtual reality.* Amsterdam: IOS Press; 2002. P. 586–592.
 52. Zardavas D, Irrthum A, Swanton C, Piccart M. Clinical management of breast cancer heterogeneity. *Nat Rev Clin Oncol.* 2015;12(7):381–394.